Structural basis for tRNA methylthiolation by the radical SAM enzyme MiaB

Authors: Olga A. Esakova[1,*], Tyler L. Grove[2,*], Neela H. Yennawar[4], Arthur J. Arcinas[3,6], Bo Wang[1], Carsten Krebs[1,3], Steven C. Almo[2], and Squire J. Booker[1,3,5*]

Affiliations: The [1]Department of Chemistry, the [3]Department of Biochemistry and Molecular Biology, [4]The Huck Institutes of the Life Sciences, and the [5]Howard Hughes Medical Institute, The Pennsylvania State University, University Park, Pennsylvania 16802, USA.

The [2]Department of Biochemistry, Albert Einstein College of Medicine, Bronx, New York

[6]Present address: AGC Biologics, Seattle, WA

Corresponding authors: squire@psu.edu, oae3@psu.edu, and tylergrove223@gmail.com

One Sentence Summary: First X-ray crystal structures of a methylthiotransferase that acts on tRNA

Summary Paragraph

Numerous post-transcriptional modifications of transfer RNAs (tRNAs) play vital roles in translation. The 2-methylthio-N^6-isopentenyladenosine (ms^2i^6A) modification occurs at position 37 (A37) in tRNAs that contain adenine in position 36 of the anticodon, and serves to promote efficient A:U codon-anticodon base-pairing and to prevent unintended base-pairing by near cognates, thus enhancing translational fidelity.[1-4] The ms^2i^6A modification is installed onto isopentenyladenosine (i^6A) by MiaB, a radical S-adenosylmethionine (SAM) methylthiotransferase (MTTase). As a radical SAM protein, MiaB contains one $[Fe_4S_4]_{RS}$ cluster used in the reductive cleavage of SAM to form a 5'-deoxyadenosyl 5'-radical (5'-dA•), which is responsible for removing the C^2 hydrogen of the substrate.[5] MiaB also contains an auxiliary $[Fe_4S_4]_{aux}$ cluster, which has been implicated in sulfur transfer to C^2 of i^6A37.[6-9] How this transfer takes place is largely unknown. Herein, we present several structures of MiaB from *Bacteroides uniformis* (*Bu*MiaB). These structures are consistent with a two-step mechanism, in which one molecule of SAM is first used to methylate a bridging μ-sulfido ion of the auxiliary cluster. In the second step, a second SAM molecule is cleaved to a 5'-dA•, which abstracts the C^2 hydrogen of the substrate, but after C^2 has undergone rehybridization from sp^2 to sp^3. This work advances our understanding of how enzymes functionalize inert C–H bonds with sulfur.

Introduction

MiaB catalyzes the final step in the biosynthesis of the hypermodified nucleoside ms^2i^6A, which is the attachment of a methylthio ($–SCH_3$) group at C^2 of i^6A37 in tRNAs that contain adenine in position 36 of the anticodon (**Fig. 1a**).[3] The human ortholog, CDK5RAP1, is mitochondrially located and responsible for modifying $Ser^{(AGN)}$, Phe, Tyr, and Trp of mitochondrial tRNAs at nucleotide i^6A37.[10,11] It also regulates the activity of the cyclin-dependent kinase 5 and is linked to functions of the central nervous system. Moreover, it is implicated in a number of cancers.[12,13] Another related class of methylthiotransferases (MTTases), designated MtaB-like [14,15], acts on C^2 of N^6-(threonylcarbamoyl)adenosine (t^6A), also found at position 37, but in $tRNA^{Lys(UUU)}$ (**Fig. 1b**). The loss of function or downregulation of one such MTTase, CDKAL1, is one of the greatest risk factors across all ethnic groups for the development of type 2 diabetes.[16] Lastly, RimO is the only known MTTase that targets a protein, which in *E. coli*, is C^3 of Asp89 of protein S12 of the 30S subunit of the bacterial ribosome (**Fig. 1c**).[17-19]

MiaB, like other known MTTases, contains an $[Fe_4S_4]_{RS}$ cluster and an $[Fe_4S_4]_{aux}$ cluster, both of which are required for its function. The $[Fe_4S_4]_{RS}$ cluster is responsible for the reductive cleavage of SAM to afford the 5'-dA•, while the $[Fe_4S_4]_{aux}$ cluster is believed to be involved in sulfur incorporation. Biochemical studies suggest that a methyl group from SAM is first transferred to an undetermined sulfur species associated with the $[Fe_4S_4]_{aux}$ cluster. Subsequently, the nascent methylthio group is transferred intact to C^2 of i^6A37 in a radical-dependent reaction.[6,20,21] Despite the importance of tRNA methylthiolation in human health,[16] how these MTTases accomplish this difficult reaction is largely unknown.

*Bu*MiaB domain architecture

*Bu*MiaB is composed of three domains (**Fig. 2a and Extended Data Table 1**): an N-terminal MTTase domain, an RS domain, and a C-terminal TRAM domain. The MTTase domain (residues 1 to 139, **Fig. S1a**) contains Cys27, Cys63 and Cys97, which coordinate three of the irons of the $[Fe_4S_4]_{aux}$ cluster (**Extended Data Fig. 3a**), while the RS domain (residues 162-396, **Fig. S1b**) exhibits a conserved core fold that consists of a shortened $(\beta\alpha)_6$ triosephosphate isomerase (TIM) barrel. The RS domain contains Cys171, Cys173 and Cys178, which coordinate three of the irons of the $[Fe_4S_4]_{RS}$ cluster. The C-terminal TRAM domain (residues 397-457, **Fig. S1c**), which was proposed to play an important role in RNA binding, is composed of a twisted antiparallel five-stranded β-sheet that is positioned over the RS domain.[22,23] The overall architecture of *Bu*MiaB is similar to that of RimO from *Thermotoga maritima* (*Tm*RimO; **PDB:4JC0**) (**Extended Data Fig. 1**). The structure of *Bu*MiaB in the absence of substrates shows that the $[Fe_4S_4]_{aux}$ and $[Fe_4S_4]_{RS}$ clusters are connected by a pentasulfide bridge (**Extended Data Fig. 1a**), as was observed in the *Tm*RimO structure.[8]

RNA interactions and binding specificity

In the structures of *Bu*MiaB complexed with a 13-mer (nucleotides 29-41) or a 17-mer (nucleotides 27-43) RNA substrate surrogate derived from the *Bacteroides uniformis* (*Bu*) $tRNA^{Phe}$ anticodon stem loop (ACSL) sequence, all three domains of the protein interact with the RNA (**Extended Data Fig. 2b**). One structure, determined to 1.5 Å resolution (**Extended Data Table 1 and Table S1**), contains *Bu*MiaB in the presence of 5'-deoxyadenosine plus methionine (5'dAH+Met) and the 13-mer. This structure shows that the central part of the enzyme contains a deep cleft (~26 Å) formed at the interface of all three domains. Two positively charged regions in the cleft are in close contact with the phosphates of the RNA backbone, forming strong

electrostatic interactions (**Extended Data Fig. 2c**). In addition, the surface of the cleft, where the 13-mer RNA is bound, contains many highly conserved amino acids (**Extended Data Fig. 2d**).

RNA bases 33 to 37 form the anticodon loop (**Extended Data Figs. 3, 4**). This loop is supported by a canonical double-stranded region exhibiting base-pairing between nucleotides 29 to 32 from the 5'-side of the RNA with nucleotides 41 to 38 on the 3'-side, respectively. This base-pairing is similar to that of full-length $tRNA^{Phe}$ in complex with MiaA (**PDB: 2ZM5**), suggesting that the tRNA maintains its native secondary structure in complex with *Bu*MiaB (**Extended Data Figs. 3a, 4a**). The RNA backbone from nucleotides 29 to 32 is contacted by a loop spanning amino acid residues 408–413 of the TRAM domain. Lys409 and Arg410 from this loop are within H-bonding distance of the RNA (**Fig. 2b, Extended Data Fig. 3b**). Arg410 supports a turn of the RNA between nucleotides G30 and C32 by electrostatic interactions with the phosphate oxygens of C32 and U33 (**Figs. 2b, 2c**). Ser446 from another loop of the TRAM domain is within H-bonding distance of the phosphate oxygen of C32. MiaB in complex with the 13-mer RNA has induced a U-turn that is not seen in the full-length tRNA in complex with MiaA (**Fig. 2b, Extended Data Figs. 3a, 4a**).[24]

U33 is conserved in all tRNAs, and our structures show a unique binding mode of this nucleotide with MiaB's TRAM domain, demonstrated to be important for substrate selection [23-25]. The U33 base is immersed in a positively charged pocket lined by Lys409, Arg410 and Lys451, conserved residues that provide selectivity for the U33 base (**Extended Data Fig. 2d**). Other residues from the pocket include Ser408 and Gln414, both of which coordinate to N^3 of U33 through a water molecule. The amide backbone nitrogen atoms of Lys409 and Arg410 form H-bonds with the C^2 oxygen atom of U33. C^5 and C^6 of U33 are in a hydrophobic interaction

with the side-chain of Val426 and the methyl group of Thr449. The side-chain of Arg410 covers the U33 binding pocket en route to interacting with the phosphate backbone (**Figs. 2b, 2c**).

Sequence analysis of tRNAs possessing ms^2i^6A37 shows a conserved adenosine at position 36, the last nucleotide of the anticodon.[15,26,27] The recognition motif for A36 is located in the β27 strand of the RS domain and includes Phe348 and Phe350, both of which form van der Waals interactions with A36. Phe348 forms an edge-to-face interaction with C^6 of A36, and Phe350 forms an edge-to-edge interaction with C^2 of A36 (**Figs. 2d, 2e**). As seen in structures of other RNA/protein complexes that recognize an adenine,[28,29] the interaction between Phe350 and C^2 of A36 may be important for base recognition. Unlike adenine, the other bases have hydrophilic groups attached to C^2 (i.e., O for C, NH_2 for U and G), which can disrupt van der Waals interactions. A36 points towards the stem of the ACSL and participates in base-stacking interactions with A38. In contrast to A36 and i^6A37, nucleotides 34 and 35, which are the first and second nucleotides of the anticodon, are not conserved in tRNAs that possess ms^2i^6A37 and do not show base-specific interactions (**Extended Data Figs. 5a, 5b**).

The immediate base after the anticodon, i^6A37, is recognized as the substrate by its isopentenyl group, which explains why MiaB only acts on A37 that has been isopentenylated.[30] The isopentenyl group makes hydrophobic contacts with the methyl groups of Thr251 and Thr252, which are connected by a cis-peptide bond needed to support these interactions (**Extended Data Fig. 5c**). The methylene groups of Cys27 and Met29 from the MTTase domain, and Leu213 and Gln215 from the RS domain, complete the hydrophobic pocket for the isopentenyl group. The only direct H-bond interaction is between the carbamoyl oxygen of Gln28 and N^6 of i^6A37. A model of *Bu*MiaB in complex with the full-length of $tRNA^{Phe}$ was constructed, revealing two regions in the MTTase domain that are potentially involved in tRNA

engagement: the highly conserved residues Gln71 and Lys72, and the positively charged loop from residues 84 to 88 (KKKKR) (**Extended Data Fig. 6**).

Active site and reaction mechanism

Two molecules of SAM are expended for each cycle of MiaB catalysis, resulting in one molecule of SAH and one molecule each of 5'-dAH and Met. The first molecule of SAM binds to the $[Fe_4S_4]_{RS}$ cluster (**Extended Data Fig. 7a**) and donates its methyl group to an acceptor, forming SAH in the process (**Fig. 4, step 1**). The most likely acceptor is a μ_2-sulfido ion from the auxiliary cluster, given its close proximity to the sulfur of SAH (4.3 Å) in the SAH-bound structure with the 13-mer RNA substrate (**Fig. 3a**), or the methyl group of SAM (3.4 Å) in the SAM-bound structure with the 17-mer (**Fig. 3b**).

The structure of *Bu*MiaB with SAM and the 17-mer represents the next snapshot in catalysis (**Fig. 3b**), which takes place after SAH leaves the active site and is replaced by a second molecule of SAM (**Fig. 4, steps 2 and 3**). The structure, obtained from crystals grown in the presence of excess SAM and the 17-mer, was determined to a resolution of 2.24 Å (**Extended Data Table 1, Table S1**). The $[Fe_3S_4]_{aux}$ cluster does not show extra density that can be attributed to a transferred methyl group, although this density would be difficult to discern at this resolution. C^2 of i^6A is 5.6 Å from the closest sulfide of the $[Fe_3S_4]_{aux}$ cluster. However, the position of i^6A changes in the structure of *Bu*MiaB co-crystallized with the 13-mer and 5'-dAH+Met. This complex mimics the step in which SAM is reductively cleaved to form the 5'-dA• and Met (**Fig. 4, steps 4, 5 and 6**). In the structure of *Bu*MiaB with the 17-mer and SAM, Arg66 is H-bonded to N^3 of i^6A (**Fig. 3b**), while in the structure with the 13-mer and 5'-dAH+Met (**Fig. 3c, Extended Data Fig. 7b**), N^3 of i^6A loses its direct interaction with Arg66

and interacts through a water molecule. The electron density around N^3 of i^6A appears to be extended in the direction of the water molecule in the structure of *Bu*MiaB with 5'dAH+Met and the 13-mer, suggesting that N^3 moves slightly out of the plane of adenosine **(Fig. 3c**).

In the structure of *Bu*MiaB with the 13-mer and 5'-dAH+Met, C^2 of i^6A sits between $C^{5'}$ of 5'-dAH and a μ_2-sulfido ion of the $[Fe_3S_4]_{aux}$ cluster at distances of 3.1 and 3.3 Å, respectively (**Fig. 3c, Extended Data Fig. 7b**). The angle between $C^{5'}$ of 5'-dAH and C^2 is 108 ± 1.5° (1.5 Å resolution) and more suitable for H-atom abstraction from an sp^3-hybridized carbon (109.5°) than from an sp^2-hybridized carbon (120°). The suggested change in hybridization at C^2 may be promoted by protonation of N^3 of i^6A by Arg66 through an intervening water molecule or by polarization of the adenine ring π-system mediated by H-bonding. Consistent with this role in catalysis, replacement of Arg66 with Gln does not inhibit methyl transfer from SAM to the cluster in solution (**Extended Data Fig. 8a**), but it does completely abolish formation of ms^2i^6A37 (**Extended Data Fig. 8b-e**).

An additional structure (1.4 Å resolution) of *Bu*MiaB in the presence of 5'-dAH+Met and the 13-mer was also determined at 1.4 Å resolution, but after pre-methylating *Bu*MiaB with SAM (**Extended Data Table 1, Table S1**). As in the previous structure of non-pre-methylated *Bu*MiaB with 5'-dAH+Met and the 13-mer, the pre-methylated *Bu*MiaB structure demonstrates distorted electron density around N^3 of i^6A (**Extended Data Fig. 9a**). We also observe extended electron density on one of the sulfides of the $[Fe_3S_4]_{aux}$ cluster, which we posit is the transferred methyl group (**Fig. 3d, Extended Data 9b)**. Such a localization of the methyl group, which might be driven by a steric clash with the i^6A substrate, necessitates that iron dissociate from the auxiliary cluster, as has recently been demonstrated spectroscopically.[7] After abstraction of the C^2 hydrogen atom, the resulting unpaired electron at C^2 is transferred into the auxiliary cluster

with concomitant rearomatization of i^6A37 (**Fig. 4, steps 7 and 8**). This step would result in reduction of an Fe^{3+} to Fe^{2+} and dissociation of the methylthio group from the fragmented auxiliary cluster, which is suggested to be $[Fe_3S_3]^{1+}$.

Discussion

We have, for the first time, determined structures of an MTTase in the presence of its macromolecular substrate. *Bu*MiaB shows exquisite selectivity for i^6A37, and various elements of the structure detail how this selectivity is achieved. Although all three domains of the protein contribute to RNA binding, the TRAM domain contributes conserved amino acids that select for U33, which is conserved in all tRNAs. A36 is found in all tRNAs that undergo the ms^2i^6A modification, and is recognized by two Phe residues contributed by the RS domain, which also select against all other nucleotides at this position. Importantly, i^6A37 is recognized predominantly by its isopentenyl modification, which is consistent with MiaB's inability to modify A37 that is not isopentenylated.

The MiaB reaction takes place in two distinct half-reactions, and it appears that one SAM binding site supports both of these steps, as has been observed for the class A RS methylases RlmN and Cfr.[31] The structure of *Bu*MiaB with bound SAM plus the 17-mer RNA substrate shows that SAM binds to the $[Fe_4S_4]_{RS}$ cluster with its methyl group positioned 3.4 Å from a bridging μ_2-sulfido ion of an $[Fe_3S_4]_{aux}$ cluster, an arrangement that is consistent with methylation of the $[Fe_3S_4]_{aux}$ cluster by a standard S_N2 mechanism. In the second half-reaction, an intact methylthio group is transferred to C^2 of i^6A37 in a radical-dependent reaction. The structure of *Bu*MiaB in the presence of the 13-mer RNA substrate and 5'-dAH+Met provides insight into how this unusual reaction takes place. C^2 of the adenine base is sandwiched between

the methylated sulfide ion of the $[Fe_3S_4]_{aux}$ cluster and the 5'-carbon of 5'-dAH at angles of ~108.5°, suggestive of tetrahedral geometry. The structure suggests that the C^2 hydrogen is abstracted upon C^2 rehybridization from sp^2 to sp^3, which would circumvent the unfavorable homolytic bond-dissociation energy associated with cleaving the C^2–H bond,[32,33] and also satisfy the spatial constraints associated with subsequent functionalization. This rehybridization is suggested to be promoted through attack at C^2 by the methylated sulfide ion of the auxiliary cluster. Our studies herein provide unprecedented insight into the mechanism of tRNA methylthiolation. A better understanding of the reaction catalyzed by RimO, and in particular how its TRAM domain is used to recognize a protein substrate, awaits better X-ray structures of that enzyme.

REFERENCES

1 Connolly, D. M. & Winkler, M. E. Genetic and physiological relationships among the miaA gene, 2-methylthio-N6-(delta 2-isopentenyl)-adenosine tRNA modification, and spontaneous mutagenesis in Escherichia coli K-12. *J. Bacteriol.* **171**, 3233-3246 (1989).

2 Connolly, D. M. & Winkler, M. E. Structure of *Escherichia coli* K-12 *miaA* and characterization of the mutator phenotype caused by miaA insertion mutations. *J. Bacteriol.* **173**, 1711-1721 (1991).

3 Esberg, B., Leung, H.-C. E., Tsui, H.-C. T., Björk, G. R. & Winkler, M. E. Identification of the miaB gene, involved in methylthiolation of isopentenylated A37 derivatives in the tRNA of Salmonella typhimurium and Escherichia coli. *J. Bacteriol.* **181**, 7256-7265 (1999).

4 Urbonavicius, J., Qian, Q., Durand, J. M. B., Hagervall, T. G. & Björk, G. R. Improvement of reading frame maintenance is a common function for several tRNA modifications. *EMBO J.* **20**, 4863–4873 (2001).

5 Arcinas, A. J. *Mechanistic Studies of the radical S-adenosyl-L-methionine (SAM) tRNA Methylthiotransferase MiaB* Ph.D. thesis, The Pennsylvania State University, (2016).

6 Landgraf, B. J., Arcinas, A. J., Lee, K.-H. & Booker, S. J. Identification of an intermediate methyl carrier in the radical S-adenosylmethionine methylthiotransferases RimO and MiaB. *J. Am. Chem. Soc.* **135**, 15404–15416 (2013).

7 Zhang, B. *et al.* First step in catalysis of the radical S-adenosylmethionine methylthiotransferase MiaB yields an intermediate with a [3Fe-4S](0)-like auxiliary cluster. *J Am Chem Soc* **142**, 1911-1924, doi:10.1021/jacs.9b11093 (2020).

8 Forouhar, F. *et al.* Two Fe-S clusters catalyze sulfur insertion by radical-SAM methylthiotransferases. *Nat. Chem. Biol.* **9**, 333–338 (2013).

9 Hernández, H. L. *et al.* MiaB, a bifunctional radical-S-adenosylmethionine enzyme involved in the thiolation and methylation of tRNA, contains two essential [4Fe–4S] clusters. *Biochemistry* **46**, 5140-5147 (2007).

10 Reiter, V. *et al.* The CDK5 repressor CDK5RAP1 is a methylthiotransferase acting on nuclear and mitochondrial RNA. *Nuc. Acids Res.* **40**, 6235–6240 (2012).

11 Wei, F. Y. *et al.* Cdk5rap1-mediated 2-methylthio modification of mitochondrial tRNAs governs protein translation and contributes to myopathy in mice and humans. *Cell Metab.* **21**, 428-442, doi:10.1016/j.cmet.2015.01.019 (2015).

12 Adami, R. & Bottai, D. S-adenosylmethionine tRNA modification: unexpected/unsuspected implications of former/new players. *Int J Biol Sci* **16**, 3018-3027, doi:10.7150/ijbs.49302 (2020).

13 Dhaven, R. & Tsai, L.-H. A decade of CDK5. *Nat. Rev. Mol. Cell Biol.* **2**, 749–759 (2001).

14 Arragain, S. *et al.* Identification of eukaryotic and prokaryotic methylthiotransferase for biosynthesis of 2-methylthio-N6-threonylcarbamoyladenosine in tRNA. *J. Biol. Chem.* **285**, 28425-28433 (2010).

15 Anton, B. P. *et al.* Functional characterization of the YmcB and YqeV tRNA methylthiotransferases of *Bacillus subtilis*. *Nucleic Acids Res.* **38**, 6195–6205 (2010).

16 Landgraf, B. J., McCarthy, E. L. & Booker, S. J. Radical S-adenosylmethionine enzymes in human health and disease. *Annu. Rev. Biochem.* **85**, 485–514, doi:10.1146/annurev-biochem-060713-035504 (2016).

17 Anton, B. P. *et al.* RimO, a MiaB-like enzyme, methylthiolates the universally conserved Asp88 residue of ribosomal protein S12 in *Escherichia coli*. *Proc. Natl. Acad. Sci. USA* **105**, 1826–1831 (2008).

18 Landgraf, B. J. & Booker, S. J. Stereochemical course of the reaction catalyzed by RimO, a radical SAM methylthiotransferase. *J Am Chem Soc* **138**, 2889-2892, doi:10.1021/jacs.5b11035 (2016).

19 Arragain, S. *et al.* Post-translational modification of ribosomal proteins: Structural and functional characterization of RimO from *Thermotoga maritima*, a radical S-adenosylmethionine methylthiotransferase. *J. Biol. Chem.* **285**, 5792–5801 (2010).

20 Agris, P. F., Armstrong, D. J., Schafer, K. P. & Soll, D. Maturation of a hypermodified nucleoside in transfer RNA. *Nucleic Acids Res.* **2**, 691-698 (1975).

21 Molle, T. *et al.* Redox Behavior of the S-Adenosylmethionine (SAM)-Binding Fe-S Cluster in Methylthiotransferase RimO, toward Understanding Dual SAM Activity. *Biochemistry* **55**, 5798-5808, doi:10.1021/acs.biochem.6b00597 (2016).

22 Lee, T. T., Agarwalla, S. & Stroud, R. M. A unique RNA Fold in the RumA-RNA-cofactor ternary complex contributes to substrate selectivity and enzymatic function. *Cell* **120**, 599-611, doi:10.1016/j.cell.2004.12.037 (2005).

23 Anantharaman, V., Koonin, E. V. & Aravind, L. TRAM, a predicted RNA-binding domain, common to tRNA uracil methylation and adenine thiolation enzymes. *Fems Microbiol Lett* **197**, 215-221, doi:10.1111/j.1574-6968.2001.tb10606.x (2001).

24 Chimnaronk, S. *et al.* Snapshots of dynamics in synthesizing N(6)-isopentenyladenosine at the tRNA anticodon. *Biochemistry* **48**, 5057-5065, doi:10.1021/bi900337d (2009).

25 Anantharaman, V., Koonin, E. V. & Aravind, L. Comparative genomics and evolution of proteins involved in RNA metabolism. *Nucleic Acids Res* **30**, 1427-1464, doi:10.1093/nar/30.7.1427 (2002).

26 Nishimura, S. *Transfer RNA: Structure, Properties, and Recognition*. 59-29 (Cold Spring Harbor Laboratory, 1979).

27 Boccaletto, P. *et al.* MODOMICS: a database of RNA modification pathways. 2017 update. *Nucleic Acids Res* **46**, D303-D307, doi:10.1093/nar/gkx1030 (2018).

28 Ellis, J. J., Broom, M. & Jones, S. Protein-RNA interactions: structural analysis and functional classes. *Proteins* **66**, 903-911, doi:10.1002/prot.21211 (2007).
29 Jones, S., Daley, D. T., Luscombe, N. M., Berman, H. M. & Thornton, J. M. Protein-RNA interactions: a structural analysis. *Nucleic Acids Res* **29**, 943-954, doi:10.1093/nar/29.4.943 (2001).
30 Pierrel, F., Douki, T., Fontecave, M. & Atta, M. MiaB protein is a bifunctional radical-S-adenosylmethionine enzyme involved in thiolation and methylation of tRNA. *J. Biol. Chem.* **279**, 47555-47653 (2004).
31 Grove, T. L., Radle, M. I., Krebs, C. & Booker, S. J. Cfr and RlmN contain a single [4Fe–4S] cluster, which directs two distinct reactivities for S-adenosylmethionine: methyl transfer by S_N2 displacement and radical generation. *J. Am. Chem. Soc.* **133**, 19586–19589 (2011).
32 Kim, S., Meehan, T. & Schaefer, H. F., III. Hydrogen-atom abstraction from the adenine–uracil base pair. *J. Phys. Chem. A.* **111**, 6806–6812 (2007).
33 Zierhut, M., Roth, W. & Fischer, I. Dynamics of H-atom loss in adenine. *Phys. Chem. Chem. Phys.* **6**, 5178–5183 (2004).

FIGURE LEGENDS

Fig. 1. Reactions catalyzed by MTTases. **a**, MiaB (CDK5RAP1). **b**, MtaB (CDKAL1). **c**, RimO. Each reaction requires two molecules of SAM, one of which is converted to SAH, and one of which is converted to 5'dAH + Met.

Fig. 2. RNA binding to *Bu*MiaB. **a**, Domains of *Bu*MiaB in complex with the 13-mer and 5'-dAH+Met in three different perspectives. The color code is the following: MTTase domain, tan; radical SAM domain, grey; TRAM domain, green. **b**, RNA recognition motifs in *Bu*MiaB. Fo-Fc omit map contoured at 3.5σ showing electron density for U33 in the recognition pocket. **c**, Electrostatic potential of the U33 binding pocket. **d**, Fo-Fc omit map (1.5 Å resolution), contoured at 3.5σ, showing the electron density for A36 interacting with conserved Phe348 and Phe350 from the radical SAM domain. **e**, Electrostatic potential in the vicinity of A36.

Fig. 3. *Bu*MiaB active site in the presence of RNA substrates. **a**, 13-mer + SAH (1.86 Å). **b**, 17-mer + SAM (2.25 Å). **c**, 13-mer + 5'dAH+Met (1.5 Å). Fo-Fc omit maps are contoured at 2.5σ in **a** and **b**, and at 3.5σ in **c**. **d**, Active site of pre-methylated *Bu*MiaB in the presence of the 13-

mer RNA and 5'dAH+Met. The electron density is a Polder map contoured at 3.0σ and shown in gray for atoms of the cluster and green for the methyl group. Panels **a**, **b**, and **c** are all distinct views; however, panel **b** is rotated clockwise ~90° from panel **a**, and panel **c** is rotated clockwise ~120° from panel **b**. Residues from the MTTase domain are colored tan, while those from the radical SAM domain are colored gray.

Fig. 4. Proposed mechanism for the MiaB reaction. One molecule of SAM binds to the $[Fe_4S_4]_{RS}$ cluster and transfers a methyl group to a bridging μ_2 sulfido ion of the auxiliary cluster (**1**). SAH dissociates and another molecule of SAM binds to the $[Fe_4S_4]_{RS}$ cluster (**2**), which is followed by tRNA binding (**3**). The methylated sulfur of the $[Fe_3S_4]_{aux}$ attacks C2 of the substrate, forming a tetrahedral intermediate (**4**). Reduction of the $[Fe_4S_4]_{RS}$ cluster (**4**) promotes formation of the 5'-dA• (**5**), which abstracts the C2 hydrogen (**6**). Loss of an electron and rearomatization of the adenine ring (**7**) leads to an $[Fe_3S_3]^{1+}$ cluster containing a methylthio ligand, which dissociates (**8**) to give the final product.

EXTENDED DATA FIGURE LEGENDS

Extended Data Fig. 1. Comparison of *Bu*MiaB and *Tm*RimO structures. a, Cartoon overlay of the structures of *Bu*MiaB (blue) and *Tm*RimO (**PDB:4JC0**) (gray). **b**, Electrostatic surface potential of *Tm*RimO (blue is positive, red is negative, and gray is neutral). **c**, Amino acid sequence alignment of *Bu*MiaB and *Tm*RimO. The overall architecture of *Bu*MiaB is similar to that of *Tm*RimO, with RMSDs of 1.5 and 1.6 Å for the two independent RimO molecules over 324 and 329 C_αs, respectively (**Table S1**). In the RimO X-ray crystal structure, the two $[Fe_4S_4]$ clusters are 7.3 Å apart (nearest ion in each cluster) and are connected by a pentasulfide bridge

spanning the unique (non-cysteinyl-ligated) irons of each cluster. This same pentasulfide bridge is observed in the *Bu*MiaB structure, wherein the clusters are 6.8 Å apart (see **Extended Data Fig. 2a**).

Extended Data Fig. 2. RNA binds to all three domains in *Bu*MiaB. a, Cartoon representation of the active site of *Bu*MiaB with a pentasulfide bridge spanning the two [Fe_4S_4] clusters. MTTase domain, tan; radical SAM domain, gray; TRAM domain, green. **b**, Cartoon of *Bu*MiaB crystallized in the presence of the 13-mer RNA substrate and 5'dAH+Met and showing the binding of the 13-mer (purple) at the interface of the three domains. **c**, Electrostatic surface potential (blue is positive, red is negative, and gray is neutral) indicates a positively charged active-site region promoting binding of the 13-mer. **d**, Conservation of amino acids in the active-site region as deduced from the CONSURF server.[34]

Extended Data Fig. 3. Comparison of ACSL structure in 13-mer bound to *Bu*MiaB with full-length $tRNA^{Phe}$ bound to *Tm*MiaA. **a**, Cartoon overlay of the 13-mer (nucleotides 29-41) structure in the complex with *Bu*MiaB and 5'-dAH+Met (purple color), with that of *Tm* $tRNA^{Phe}$ in complex with MiaA (tan color) (**PDB ID: 2ZM5**). **b**, Schematic diagram of hydrogen bonds formed between the 13-mer and *Bu*MiaB.

Extended Data Fig. 4. Comparison of ACSL structure in 17-mer bound to *Bu*MiaB with full-length $tRNA^{Phe}$ bound to *Tm*MiaA. a, Cartoon overlay of the 13-mer (purple color) and 17-mer (nucleotides 27-43) (green color) structures in complex with *Bu*MiaB plus 5'-dAH+Met (13-mer) or *Bu*MiaB with SAM (17-mer), with that of *Tm* $tRNA^{Phe}$ in complex with MiaA (tan color) (**PDB ID: 2ZM5**). **b**, Schematic diagram of the H-bonds formed between the 17-mer and *Bu*MiaB.

Extended Data Fig. 5. Active site interactions of *Bu*MiaB with nucleotides 34 and 35 of the anticodon. The structure of *Bu*MiaB with the 13-mer RNA and 5'dAH+Met is shown in pink, while the structure of *Bu*MiaB with the 17-mer RNA and SAM is shown in maroon. **a**, Active site interactions with G34. G34 is often modified, and its base inserts between the TRAM and RS domains in a deep cleft, which provides space for modifications. In the structure of *Bu*MiaB in complex with 5'-dAH+Met and the 13-mer, N^{10} of G34 is within H-bonding distance to Ser388 of the RS domain. The 2' and 3' OH groups are H-bonded to two nitrogen atoms from the guanidinium group of Arg418 from the TRAM-domain. In the structure of *Bu*MiaB with SAM and the 17-mer, the position of G34 is different, and the base no longer interacts with Ser388 and Arg418 (**Extended Data Figs. 3b, 4b**). **b**, Active site interactions with A35. In the structure of *Bu*MiaB with 5'-dAH+Met and the 13-mer, the carboxylate oxygens of Asp319 are within H-bonding distance to N^6 of A35, while the side-chain of Gln28 is in H-bonding distance to the 2' OH of A35. The A35 base is π-stacked between Phe348 on one side and the adenine ring of i^6A37 on the other. The position of A35 is shifted in the SAM-bound structure and is stabilized by π-stacking with G34 on one side and Phe348 on the other. The rotation of Phe348 supports two different orientations of A35 in the active site of the enzyme. **c**, Binding of i^6A37 in the active site of *Bu*MiaB in the structure with the 13-mer and 5'dAH+Met, showing that the isopentenyl group sits in a hydrophobic patch. All figures have the same color for the domains and their associated residues: tan for MTTase, gray for radical SAM and green for TRAM.

Extended Data Fig. 6. A Model for full-length tRNA binding to *Bu*MiaB. a, Conservation of residues in *Bu*MiaB as deduced from the CONSURF server. The color code is described in the panel. **b**, Electrostatic surface potential, indicating positively charged regions that could stabilize

375 $tRNA^{Phe}$. **c**, A predicted model of interactions between the residues from the MTTase domain
376 and the full-length tRNA.

377 **Extended Data Fig. 7. Binding of SAM, SAH, and 5'-dAH to *Bu*MiaB**. **a**, Overlay of SAM
378 (gray), SAH (aquamarine) and 5'dAH+Met (light violet) in their complexes with *Bu*MiaB and
379 RNA substrates (17-mer for SAM, and 13-mer for SAH or 5'-dAH+Met). The adenine ring of
380 SAM, SAH and 5'dAH forms face-to-face π-stacking interactions with Phe321. This stacking is
381 further supported by edge-to-face interactions with two tyrosines (177, 352) and Phe350. N^3 of
382 the adenine ring H-bonds with the conserved Arg66 (shown in **Fig. 3a**), and N^6 forms three H-
383 bonds with the carbonyl groups of Ile65 (MTTase domain), and Tyr177 and Ser353 (RS
384 domain). The ribose moiety of SAM, SAH and 5'dAH H-bonds with Arg66, Gln281 and
385 Asp319. Methionine in the 5'dAH+Met structure or the methionine moiety of SAM (with the 17-
386 mer RNA) and SAH (with 13-mer RNA) in structures with those molecules bound shows the
387 canonical bidentate binding to the unique iron of the $[Fe_4S_4]_{RS}$ cluster. **b**, Overlay of SAM (gray)
388 or 5'dAH+Met (light violet) in complex with *Bu*MiaB and the 17-mer RNA (SAM) or 13-mer
389 RNA (5'-dAH+Met). The i^6A37 base is in pink for the structure with 5'dAH+Met and maroon
390 for the structure with SAM. All figures have the same color for the domains and their associated
391 residues: tan for MTTase, gray for radical SAM and green for TRAM, except for Gln215 in the
392 structure with 5'dAH+Met (panel a), which rotates.

393 **Extended Data Fig. 8. Effect of Arg66→Gln substitution on *Bu*MiaB activity**. **a**, Time
394 course for SAH formation upon incubating 25 μM *Bu*MiaB WT (black circles) or *Bu*MiaB R66Q
395 (red circles) with 1 mM SAM in the absence of dithionite. **b-e**, Time course for formation of
396 SAH (**b**), 5'dAH (**c**), ms^2i^6A (**d**), and decay of i^6A (**e**), after 30 min of initial incubation of 25 μM
397 *Bu*MiaB with 1 mM SAM followed by addition of 100 μM i^6A ACSL RNA and reaction

initiation with 1 mM dithionite. The black color corresponds to data obtained for *Bu*MiaB WT in the presence of the 17-mer RNA substrate; the blue color corresponds to data obtained in the presence of the 13-mer; and the red color corresponds to data for *Bu*MiaB R66Q in the presence of the 17-mer. Error bars represent one standard deviation for reactions conducted in triplicate, with the centre representing the mean.

Extended Data Fig. 9. Stereoscopic representation of the active site electron density of pre-methylated *Bu*MiaB in the presence of the 13-mer RNA substrate and 5'dAH+Met. The structure of *Bu*MiaB does not show any significant changes in the protein or RNA components of the complex in the pre-methylated versus non-pre-methylated states [RMSD = 0.231 Å (C_α = 371 atoms) and 0.089 Å (C_α = 439 atoms) for pre-methylated subunits A and B, respectively, versus non-pre-methylated subunit A; and 0.092 Å (C_α = 415 atoms) and 0.248 Å (C_α = 392 atoms) for pre-methylated subunits A and B, respectively, versus non-methylated subunit B]. **a**, The extended electron density at N^3. The gray mesh corresponds to an Fo-Fc omit map for i^6A contoured at 3.5σ, and the green mesh to an Fo-Fc map contoured at 3.0σ after refinement with i^6A. **b**, The extended electron density at the sulfur atom of the [Fe_3S_4] cluster. The mesh corresponds to an Fo-Fc omit map for the methyl group (green color) attached to the sulfur (gray color) of the auxiliary cluster contoured at 3.5σ. **c**, In a map generated for the non-pre-methylated auxiliary cluster, no extended density is observed. The mesh corresponds to an Fo-Fc omit map for the sulfur atom of the auxiliary cluster contoured at 3.5σ. All residues have a common color theme for the domains: tan for MTTase and gray for radical SAM.

Extended Data Table 1. X-ray crystallographic data collection and refinement statistics. *Values in parentheses represent the highest-resolution shell.

METHODS

Cloning of the gene encoding *Bu*MiaB (native *Bu*MiaB structure)

The gene encoding *Bu*MiaB (Uniprot: A7UYY7) was amplified from *Bacteroides uniformis (strain ATCC 8492)* genomic DNA using the following forward and reverse primers, respectively: 5'-TACTTCCAATCCATGATGGAAAAAGTAACGGGAGCAGAC-3' and 5'-TATCCACCTTTACTGTTAGCCGGCTACCTCTTCTCCTTTC-3'. The PCR products were purified with the Agencourt Ampure XP PCR clean-up kit (Beckman Coulter) using the manufacturer's protocol. The pSGC vector was prepared for ligation-independent cloning (LIC) by linearization with the restriction enzyme *Bsa*I. LIC sites were installed by adding T4 DNA polymerase (New England Biolabs, NEB) to 10 μg linearized plasmid in a 50 μL reaction containing 2.5 mM GTP, 1× NEB Buffer 2, and 1× bovine serum albumin (BSA) for 1 h at 22 ° C. T4 DNA polymerase was heat-inactivated by incubation at 75 °C for 20 min. 2 μL of the PCR products were also treated with T4 DNA polymerase in a 10 μL reaction containing 2.5 mM CTP, 1× NEB Buffer 2, and 1× BSA for 1 h at 22 ° C. T4 DNA polymerase was heat inactivated by incubation at 75 °C for 20 min. The LIC reaction was carried out by mixing 15 ng of digested vector with ~ 40 ng of digested PCR product with a subsequent incubation at 22 °C for 10 min. A 30 μL aliquot of DH10B cells (NEB) was used in a transformation along with 2 μL of the above mixture using standard protocols. Cloning the genes into pSGC with this method adds a hexahistidine tag with a TEV cleavage site to the N-terminus of the protein (MHHHHHHSSGVDLGTENLYFQS-protein). All final constructs were sequence-verified with dideoxy sequencing performed by Genescript. For expression, *E. coli* BL21(DE3) cells containing the pDB1282 plasmid were transformed with the above construct.[35] Transformants were selected on an LB agar plate containing 50 μg/mL kanamycin and 100 μg/mL ampicillin. A

single colony was used to inoculate 20 mL of LB which, after overnight incubation, was used to start 2 L of super broth expression media in a 2 L PYREX® media bottle. After 5 h of growth at 37 °C, cysteine and arabinose were added to final concentrations of 600 and 0.1 %, respectively. The cultures were incubated for an additional hour before being cooled to 22 °C. After ~ 20 h, the cells were harvested by centrifugation at 10,000 ×*g*, flash frozen, and stored in liquid nitrogen until purification.

Cloning and expression of the gene encoding *Bu*MiaB (substrate-bound structures)

The second gene encoding *Bu*MiaB **(A0A174NUT3)** was synthesized by GeneArt Life-technologies (www.lifetechnologies.com) (see supporting information for DNA and protein sequence) and was provided in a pMAT-plasmid inserted using *Nde*I and *Eco*RI restriction sites. The pMAT-*Bu*MiaB plasmid was digested with *Nde*I and *Eco*RI and ligated into a similarly digested pET-28a plasmid by standard procedures.[36] The correct construct, which encodes MiaB containing an N-terminal hexahistidine tag separated from the native initial amino acid by a spacer of 10 aa, was verified by sequencing at the Penn State (University Park) Huck Genomics Core facility. The resulting expression vector, pET28-*Bu*MiaB, was used along with plasmid pDB1282 to transform *E. coli* BL21 (DE3) as previously described.[35,37] The encoded protein differs from the one used for the native *Bu*MiaB structure by one amino acid change: A0A174NUT3 contains His at position 363, while A7UYY7 contains Tyr.

Bacterial growth and gene expression were carried out at 37 °C in 16 L of LB media distributed evenly among 4 Erlenmeyer flasks with moderate shaking (180 rpm). At an optical density (OD) of 0.3 at 600 nm (OD_{600}), solid *L*-(+)-arabinose was added to each flask to a final concentration of 0.2 % (w/v), while cysteine and ferric chloride were added to final

concentrations of 300 μM and 50 μM, respectively. At an OD_{600} of 0.6, solid isopropyl β-D-thiogalactopyranoside (IPTG) was added to each flask to a final concentration of 500 μM. Expression was allowed to take place for 16 h at 18 °C before the cells were harvested by centrifugation at 7,000 × g for 12 min at ambient temperature. The cell paste was frozen and stored under liquid nitrogen.

Purification of *Bu*MiaB

*Bu*MiaB was purified under anoxic conditions in a Coy (Grass Lakes, MI) anaerobic glovebox, which was filled with a mixture of N_2 (95%) and H_2 (5%) and maintained below 1 ppm O_2 using palladium catalysts. *Bu*MiaB was purified by immobilized metal affinity chromatography (IMAC) using Ni-NTA resin (Qiagen). 30 g cell paste was suspended in 100 mL lysis buffer (50 mM HEPES, pH 7.5, 300 mM KCl, 10 mM $MgCl_2$, 10 mM 2-mercaptoethanol, 10 mM imidazole, 1 mg/mL lysozyme), placed in a metal cup, and incubated in an ice-water bath for 30 min. The cells were then subjected to a series of bursts of sonic disruption in the glovebox while maintaining the cell suspension at ≤ 8 °C. The cell suspension was transferred into sterile centrifuge tubes, which were subsequently sealed, removed from the anaerobic chamber and centrifuged at 45,000 × g for 1 h at 4 C°. The supernatant was loaded onto a Ni-NTA column (30 ml), which was subsequently washed with an appropriate volume of wash buffer (50 mM HEPES, pH 7.5, 300 mM KCl, 10 mM $MgCl_2$, 10 mM 2-mercaptoethanol, 20 mM imidazole). *Bu*MiaB was eluted from the resin using elution buffer (50 mM HEPES, pH 7.5, 300 mM KCl, 10 mM $MgCl_2$, 10 mM 2-mercaptoethanol, 250 mM imidazole). Fractions containing *Bu*MiaB, distinguished by their dark brown color, were pooled and concentrated using Amicon Ultracel – 10 K centrifugal filters (Millipore, Billerica,MA). The protein was

exchanged into storage buffer (50 mM HEPES, pH 7.5, 150 mM KCl, 20% glycerol, 10 mM $MgCl_2$, 1 mM DTT), snap frozen in small aliquots in liquid nitrogen and stored under liquid nitrogen.

To ensure complete Fe/S cluster content, *Bu*MiaB (0.1 mM) was subjected to reconstitution by incubating it with an 8-fold molar excess of $FeCl_3$ and Na_2S, at 4 ˚C overnight, as described previously.[35,37] The protein was concentrated using centrifugal filters and applied to an S-200 size-exclusion column connected to an ÄKTA liquid chromatography system (GE Biosciences) housed in an anaerobic glovebox. The column was equilibrated in storage buffer at a flow rate of 0.5 ml/min before injecting the protein and eluting it at the same flow rate. Fractions were chosen based on their brown color, elution time and having both an absorbance at 280 nm (protein) and at 400 nm (Fe/S cluster).

Preparation of RNA substrates

An oligoribonucleotide substrate corresponding to the 17-nucleotide (17-mer) anticodon stem-loop (ACSL) of *Bu* $tRNA^{Phe}$ (5'-AAGGACUGAA**A**AUCCUU-3') was synthesized by Dharmacon Thermo Fisher Scientific (Lafayette, CO). Nucleotide A37, shown in bold, is the site of modification by MiaA and MiaB. *E. coli* MiaA was used to transfer a dimethylallyl group from dimethylallyl pyrophosphate to N^6 of A37 as described previously.[6] A 13-mer from the ACSL of *Bu* $tRNA^{Phe}$ (5'-GGACUGAA(i6)**A**AUCC-3') was also synthesized by Dharmacon Thermo Fisher Scientific. In this instance, the i^6A modified based was synthesized chemically, as described previously,[6] and then supplied to Dharmacon for incorporation into the oligonucleotide.

Crystallization of native *Bu*MiaB

Diffraction-quality crystals of *Bu*MiaB were obtained by the sitting-drop vapor diffusion method at 20 °C in an anaerobic chamber maintained at < 0.1 ppm oxygen (MBraun, Stratham, NH). Drops of 0.4 µL protein solution (TEV-cleaved *Bu*MiaB diluted to 5 mg•mL^{-1} in 10 mM HEPES, pH 7.5, 10 mM DTT) were mixed with 0.4 µL precipitant (0.2 M potassium formate, pH 7.3, 20% polyethylene glycol 3350) and equilibrated against a solution of 0.5 M LiCl. The crystals were mounted directly from the drops with nylon loops and flash-cooled in liquid nitrogen inside the anaerobic chamber, and stored in liquid nitrogen prior to data collection. Diffraction data were collected at the Advanced Photon Source (Argonne National Laboratory, Argonne IL) on beamline 23-ID-D (GMCA) at 100 K and were integrated and scaled using HKL3000 [38] A 2.06 Å resolution dataset was collected at a wavelength of 1.078 Å. Phases were determined by molecular replacement using RimO (PDB 2QGQ) as the search model.[8] This initial model was then refined with rounds of automated model building performed by Phenix AutoBuild,[39] interspersed with manual model building and refinement using Coot,[40] phenix.refine.[41] The final model comprises a single polypeptide chain containing amino acid residues 16 to 65 and 72 to 457 out of a total of 457 residues. The model also contains 2 [Fe_4S_4] clusters, a Mg^{2+} ion, and a pentasulfide bridge. Validation of the model was performed with MolProbity.[42] The Ramachandran plot shows that 97.4% of residues are in favored regions, with the remaining 1.6% in allowed regions. Full data processing, refinement, and validation details are in **Extended Data Table 1**.

Crystallization of *Bu*MiaB in the presence of substrates

535 *Bu*MiaB (10 mg/mL), in a buffer containing 15 mM HEPES, pH 7.5, 100 mM KCl, 5
536 mM DTT and 10 mM $MgCl_2$, was incubated at room temperature first with 1 mM SAM for 30
537 min, and subsequently with a 1:1.3 ratio of *Bu*MiaB to the 17-mer RNA substrate for 30
538 additional min. The solution of the protein/RNA complex was passed through a 0.2 μm sterile
539 centrifugal filter (EMD Millipore, Billerica, MA). Crystals of the complex were obtained from
540 100 mM Na-cacodylate, pH 5.5, 13% PEG 4000 and 3% (+/-)-2-methyl-2,4-pentanediol or 1%
541 of 1,2-butanediol as additives, which was also used in the well, with the exception of the (+/-)-2-
542 methyl-2,4-pentanediol or 1% of 1,2-butanediol. Diffraction datasets were collected at the
543 Advanced Photon Source (Argonne National Laboratory, Argonne IL) on beamline 23-ID-B
544 (GMCA) at 100 K and at a wavelength of 1.033 Å. The Ramachandran plot shows that 97.4% of
545 residues are in favored regions, with 3.4% in allowed regions and 0.2% as outliers.

546 To generate the *Bu*MiaB complex with RNA+SAH, *Bu*MiaB was first incubated with 1
547 mM SAH for 30 min, and subsequently with a 1:1.3 ratio of *Bu*MiaB with the 17-mer or 13-mer
548 RNA RNA substrate for 30 additional min. Crystals exhibiting the best diffraction grew in three
549 days from the condition containing 100 mM Na-cacodylate, pH 5.5, 13% PEG 4000 and 3% 1,6-
550 hexanediol, which was also used in the well, with the exception of the 1,6-hexanediol.
551 Diffraction datasets were collected at the Advanced Photon Source (Argonne National
552 Laboratory, Argonne IL) on beamline 23-ID-B (GMCA) at 100 K and at a wavelength of 1.033
553 Å. The Ramachandran plot shows that 98.2% of residues are in favored regions, with the
554 remaining 1.8% in allowed regions.

555 The crystallization conditions for the complex of *Bu*MiaB with the 13-mer and
556 5'dAH+Met were the same as those for the *Bu*MiaB structure with SAM and the 17-mer.
557 *Bu*MiaB was first incubated with methionine for 15 min, and subsequently with 5'-dAH for 30

558 min, before incubating it with a 1:1.3 ratio of the protein to the 13-mer for 30 min. Diffraction
559 datasets were collected at the Advanced Photon Source (Argonne National Laboratory, Argonne
560 IL) on beamline 23-ID-B (GMCA) at 100 K and at a wavelength of 1.033 Å. The Ramachandran
561 plot shows that 97.6% of residues are in favored regions, with the remaining 2.4% in allowed
562 regions.

563

564 **Crystallization of pre-methylated *Bu*MiaB**

565 *Bu*MiaB (200 μM) was incubated with 1 mM SAM for 45 min, and then excess SAM
566 was removed by gel-filtration chromatography. This protein was then mixed with 5 mM Met, 1
567 mM 5'-dAH and the 13-mer RNA substrate (250 μM) for crystallization. Crystals formed in
568 three days in the same crystallographic conditions as for the non-methylated enzyme. Diffraction
569 datasets were collected at the Advanced Photon Source (Argonne National Laboratory, Argonne
570 IL) on beamline 23-ID-B (GMCA) at 100 K and at a wavelength of 1.033 Å. The structure of the
571 pre-methylated *Bu*MiaB with 5'-dAH+Met and the 13-mer RNA was determined at a resolution
572 of 1.4 Å. A Ramachandran plot of the final model shows that 97.6% of residues are in favored
573 regions, with the remaining 2.4% in allowed regions (**Extended Data Table 1**). The structure
574 does not show any significant changes in the protein or RNA components of the complex in the
575 methylated versus unmethylated states [RMSD = 0.231 Å (C_α = 371 atoms) and 0.089 Å (C_α =
576 439 atoms) for methylated subunits A and B, respectively, versus unmethylated subunit A; and
577 0.092 Å (C_α = 415 atoms) and 0.248 Å (C_α = 392 atoms) for methylated subunits A and B,
578 respectively, versus unmethylated subunit B].

579

Modeling of *Bu*MiaB with full-length tRNA

The crystal structures of *Bu*MiaB with 5'-dAH+Met and the bound 13-mer RNA substrate were used as a guide for building a model of the complex of *Bu*MiaB with the full-length tRNA. The structure of the tRNA-modifying enzyme MiaA in complex with $tRNA^{Phe}$ (**PDB: 2ZM5**) served as the starting model. The ACSL base-pairing within the helical stem of the full-length tRNA was aligned onto the 13-mer RNA in the structure of *Bu*MiaB with 5'-dAH+Met. The model of the $tRNA^{Phe}$+*Bu*MiaB complex was guided by conserved residues and positive electrostatic surface potential favorable for the RNA phosphate backbone contacts (**Fig. S7**).

Generation of the Arg66Gln *Bu*MiaB variant and subsequent activity measurements

The Arg66Gln variant of *Bu*MiaB was generated using the Stratagene Quikchange site-directed mutagenesis kit according to the manufacturer's protocol. The pET28-*Bu*MiaB construct was used as a template in conjunction with a forward primer (5'-GAATACCTGTAGCATTCAGGATAACGCCGAACAG-3') and a reverse primer (5'-CTGTTCGGCGTTATCCTGAATGCTACAGGTATTC-3'). Activity measurements of *Bu*MiaB WT and *Bu*MiaB-R66Q were conducted as previously described using the 17-mer or 13-mer oligonucleotide substrate from the ACSL of *Bu* $tRNA^{Phe}$ (**Fig. S9**).[6]

ADDITIONAL REFERENCES

34 Ashkenazy, H. *et al.* ConSurf 2016: an improved methodology to estimate and visualize evolutionary conservation in macromolecules. *Nucleic Acids Res* **44**, W344-350, doi:10.1093/nar/gkw408 (2016).

35 Lanz, N. D. *et al.* RlmN and AtsB as models for the overproduction and characterization of radical SAM proteins. *Methods Enzymol.* **516**, 125-152, doi:10.1016/B978-0-12-394291-3.00030-7 (2012).
36 Sambrook, J., Fritsch, E. F. & Maniatis, T. *Molecular Cloning: A Laboratory Manual*. 2nd edn, Vol. 3 (Cold Spring Harbor Laboratory Press, 1989).
37 McCarthy, E. L. & Booker, S. J. Biochemical approaches for understanding iron-sulfur cluster regeneration in *Escherichia coli* lipoyl synthase during catalysis. *Methods Enzymol* **606**, 217-239 (2018).
38 Minor, W., Cymborowski, M., Otwinowski, Z. & Chruszcz, M. HKL-3000: the integration of data reduction and structure solution--from diffraction images to an initial model in minutes. *Acta crystallographica. Section D, Biological crystallography* **62**, 859-866, doi:10.1107/S0907444906019949 (2006).
39 Terwilliger, T. C. *et al.* Iterative model building, structure refinement and density modification with the PHENIX AutoBuild wizard. *Acta crystallographica. Section D, Biological crystallography* **64**, 61-69, doi:10.1107/S090744490705024X (2008).
40 Emsley, P., Lohkamp, B., Scott, W. G. & Cowtan, K. Features and development of Coot. *Acta Crystallogr. D Biol. Crystallogr.* **66**, 486–501 (2010).
41 Afonine, P. V. *et al.* Towards automated crystallographic structure refinement with phenix.refine. *Acta crystallographica. Section D, Biological crystallography* **68**, 352-367, doi:10.1107/S0907444912001308 (2012).
42 Williams, C. J. *et al.* MolProbity: More and better reference data for improved all-atom structure validation. *Protein Sci* **27**, 293-315, doi:10.1002/pro.3330 (2018).

ACKNOWLEDGMENTS

Funding Sources

This work was supported by NIH (GM-122595 to S.J.B; AI133329, to S.C.A. and T.L.G.; GM-127079 to C.K.; and GM118393, GM093342, and GM094662 to S.C.A.), NSF (MCB-1716686 to S.J.B.), the Eberly Family Distinguished Chair in Science (S.J.B.), The Price Family Foundation (S.C.A), and the Penn State Huck Institutes of the Life Sciences (N.H.Y.). S.J.B. is an investigator of the Howard Hughes Medical Institute. This research used resources of the Advanced Photon Source, a U.S. Department of Energy (DOE) Office of Science User Facility operated for the DOE Office of Science by Argonne National Laboratory under Contract No.

DE-AC02-06CH11357. Use of GM/CA@APS has been funded in whole or in part with Federal funds from the National Cancer Institute (ACB-12002) and the National Institute of General Medical Sciences (AGM-12006). The Eiger 16M detector at GM/CA-XSD was funded by NIH grant S10 OD012289. Use of the LS-CAT Sector 21 was supported by the Michigan Economic Development Corporation and the Michigan Technology Tri-Corridor (Grant 085P1000817). This research also used the resources of the Berkeley Center for Structural Biology supported in part by the Howard Hughes Medical Institute. The Advanced Light Source is a Department of Energy Office of Science User Facility under Contract No. DE-AC02-05CH11231. The ALS-ENABLE beamlines are supported in part by the National Institutes of Health, National Institute of General Medical Sciences, grant P30 GM124169.

Author contributions: O.A.E., T.L.G., N.H.Y., and S.J.B. developed the research plan and experimental strategy. O.A.E. and T.L.G. isolated and crystallized proteins and collected crystallographic data. O.A.E., B.W., and A.J.A. performed biochemical experiments. O.A.E., T.L.G., N.H.Y., S.C.A. C.K. and S.J.B. analyzed and interpreted crystallographic data. O.A.E., T.L.G., N.H.Y., and S.J.B. wrote the manuscript, while all other authors reviewed and commented on it.

The authors declare no competing interests

Additional Information: supplementary information is available for this paper.

Correspondence and requests for materials should be addressed to Squire J. Booker (squire@psu.edu)

Data Availability: Atomic coordinates and structure factors for the reported crystal structures in this work have been deposited to the Protein Data Bank (PDB) under accession numbers 7MJZ (native structure with pentasulfide bridge), 7MJY (structure with SAH and 13-mer RNA), 7MJV (structure with SAM and 17-mer RNA), 7MJX (structure with 5'-dAH+Met and 13-mer RNA), and 7MJW (structure with pre-methylated *Bu*MiaB and 5'-dAH+Met and 13-mer RNA).

ORCID

Squire J. Booker: 0000-0002-7211-5937

Olga A. Esakova: 0000-0001-8377-8368

Tyler L. Grove: 0000-0002-4763-0646

Arthur J. Arcinas: 0000-0003-4903-3500

Steven C. Almo: 0000-0003-2591-5234

Bo Wang: 0000-0002-0381-3686

Neela H. Yennawar: 0000-0001-7278-659X

Carsten Krebs: 0000-0002-3302-7053

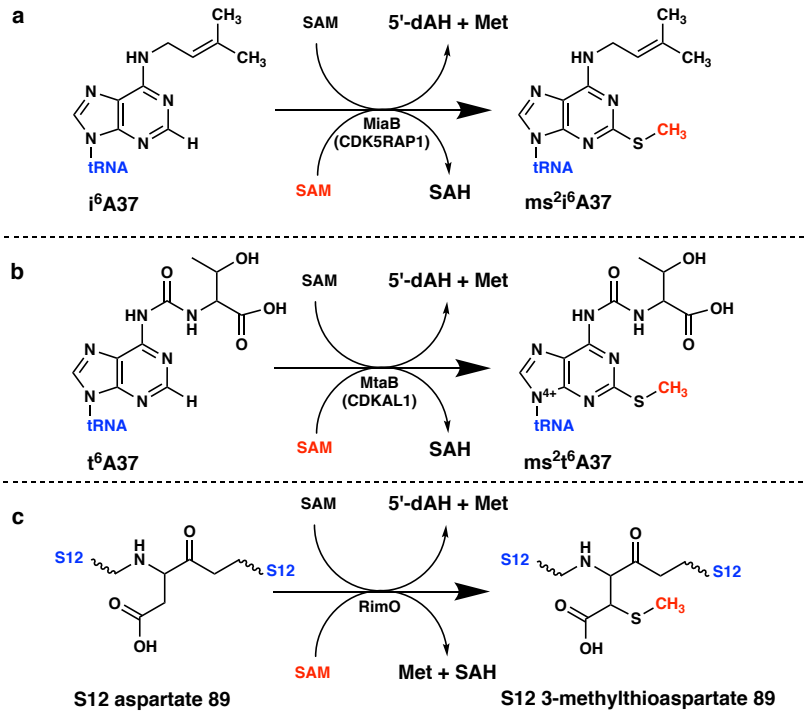
a
SAM
5'-dAH + Met
MiaB
(CDK5RAP1)
SAM
SAH
tRNA
i6A37
ms2i6A37
b
SAM
5'-dAH + Met
MtaB
(CDKAL1)
SAM
SAH
t6A37
ms2t6A37
c
SAM
5'-dAH + Met
RimO
SAM
Met + SAH
S12
S12 aspartate 89
S12 3-methylthioaspartate 89

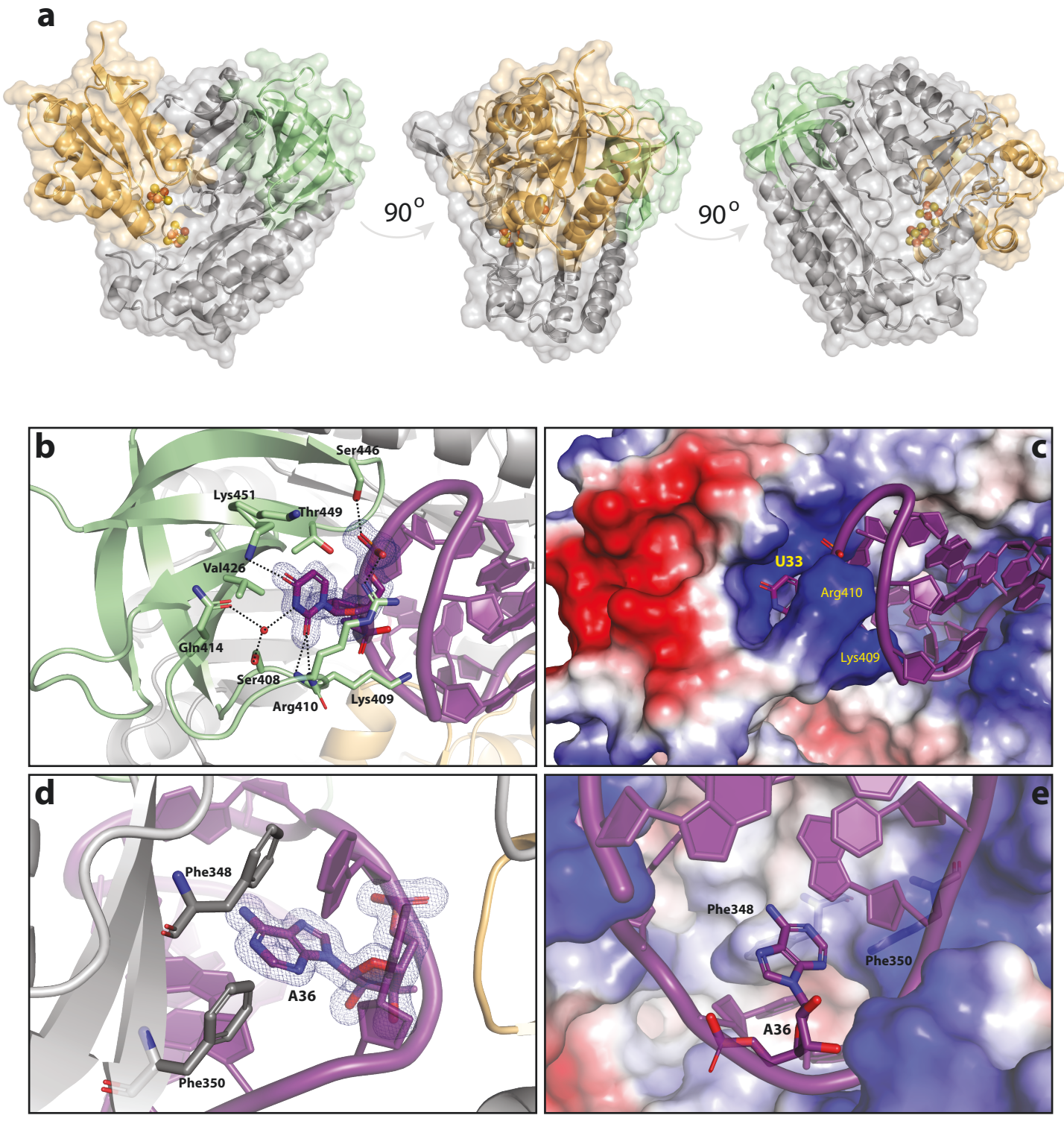
a
90°
90°
b
Ser446
Lys451
Thr449
Val426
Gln414
Ser408
Arg410
Lys409
c
U33
Arg410
Lys409
d
Phe348
A36
Phe350
e
Phe348
Phe350
A36

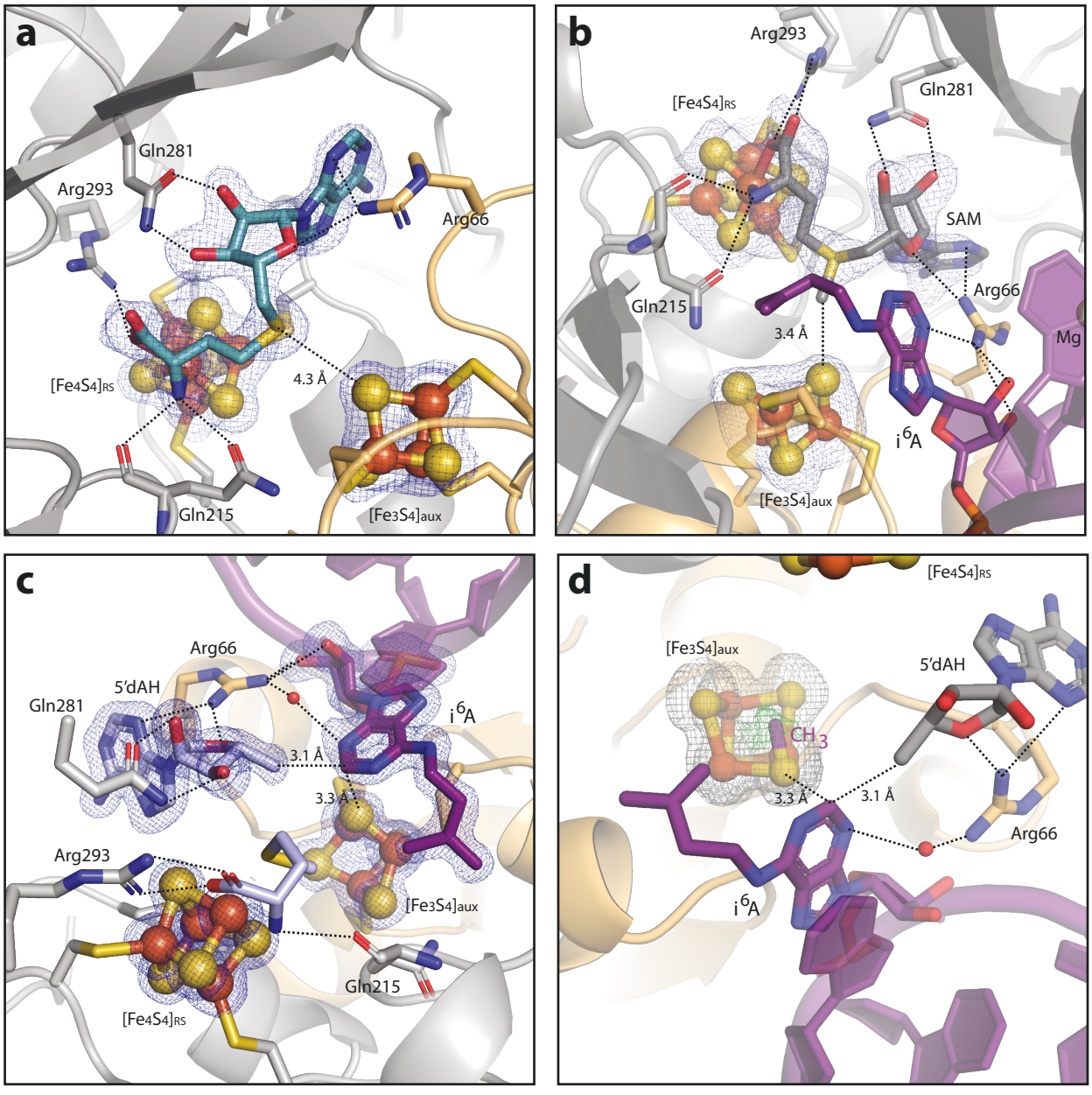
a
Gln281
Arg293
Arg66
[Fe4S4]RS
4.3 Å
Gln215
[Fe3S4]aux
b
Arg293
[Fe4S4]RS
Gln281
SAM
Gln215
Arg66
3.4 Å
Mg
i6A
[Fe3S4]aux
c
Arg66
5′dAH
Gln281
i6A
3.1 Å
3.3 Å
Arg293
[Fe3S4]aux
Gln215
[Fe4S4]RS
d
[Fe4S4]RS
[Fe3S4]aux
5′dAH
CH3
3.3 Å
3.1 Å
Arg66
i6A

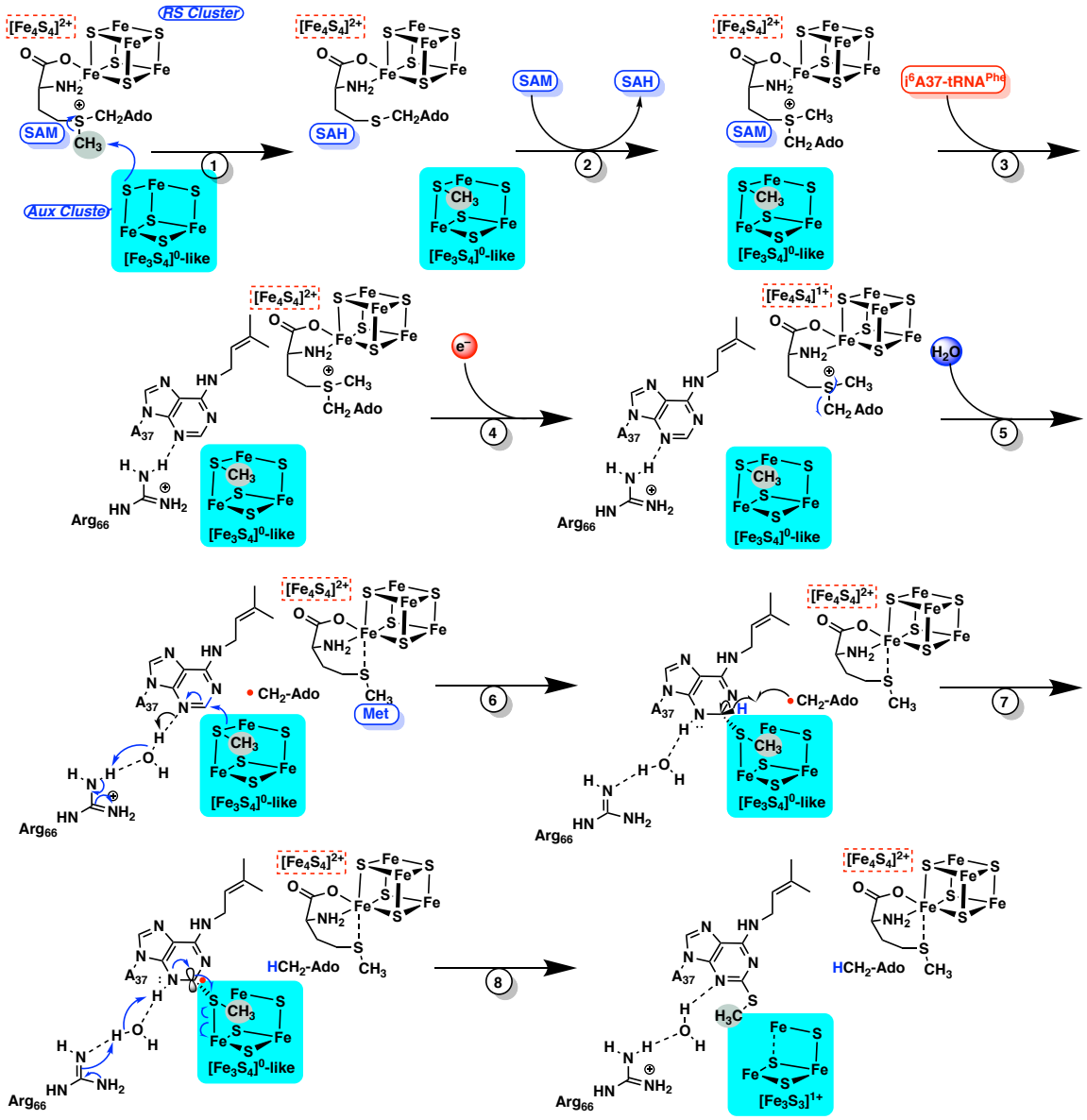
RS Cluster
[Fe4S4]2+
SAM
SAH
Aux Cluster
[Fe3S4]0-like
[Fe4S4]1+
i6A37-tRNAPhe
e−
H2O
CH2 Ado
CH2-Ado
HCH2-Ado
Met
Arg66
A37
[Fe3S3]1+
1
2
3
4
5
6
7
8

Supplementary Information for

"Structural basis for tRNA methylthiolation by the radical SAM enzyme MiaB"

Authors: Olga A. Esakova[1,*], Tyler L. Grove[2,*], Neela H. Yennawar[4], Arthur J. Arcinas[3,6], Bo Wang[1], Carsten Krebs[1,3], Steven C. Almo[2], and Squire J. Booker[1,3,5*]

Affiliations: The [1]Department of Chemistry, the [3]Department of Biochemistry and Molecular Biology, [4]The Huck Institutes of the Life Sciences, and the [5]Howard Hughes Medical Institute, The Pennsylvania State University, University Park, Pennsylvania 16802, USA.

The [2]Department of Biochemistry, Albert Einstein College of Medicine, Bronx, New York

[6]Present address: AGC Biologics, Seattle, WA

Corresponding authors: squire@psu.edu, oae3@psu.edu, and tylergrove223@gmail.com

Table of Contents

Table S1: The root mean square deviation (RMSD) for each model against the structure of *Bu*MiaB with a pentasulfide was calculated using The PyMOL Molecular Graphics System, Version 2.0 Schrödinger, LLC

.

Structure	PDB entry	Chain	RMSD (Å) *Main chain*
Bacteroides uniformis MiaB with pentasulfide bridge	7MJZ	A	reference
Thermatoga maritima RimO	4JC0	A B	1.6 1.5
Bacteroides uniformis MiaB co-crystallized with SAH and 13-mer ACSL $tRNA^{Phe}$	7MJY	A	0.4
Bacteroides uniformis MiaB co-crystallized with SAM and 17-mer ACSL $tRNA^{Phe}$	7MJV	A	0.4
Bacteroides uniformis MiaB co-crystallized with 5'dAH+Met and 13-mer ACSL $tRNA^{Phe}$	7MJX	A B	0.9 1.0
Methylated *Bacteroides uniformis* MiaB co-crystallized with 5'dAH+Met and 13-mer ACSL $tRNA^{Phe}$	7MJW	A B	1.0 0.9

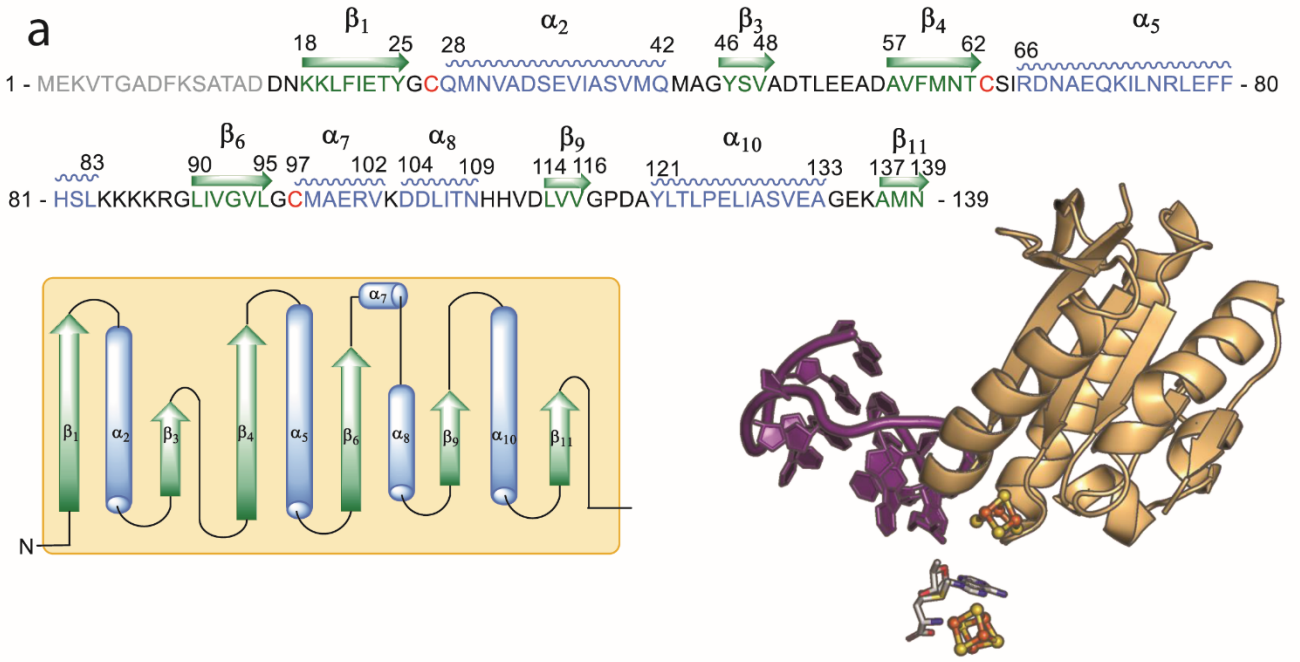
a
β1 18 25
α2 28 42
β3 46 48
β4 57 62
α5 66
1 - MEKVTGADFKSATAD DNKKLFIETYGCQMNVADSEVIASVMQ MAGYSVADTLEEADAVFMNTCSIRDNAEQKILNRLEFF - 80
β6 83 90 95
α7 97 102
α8 104 109
β9 114 116
α10 121 133
β11 137 139
81 - HSLKKKKRGLIVGVLGCMAERVKDDLITNHHVDLVVGPDAYLTLPELIASVEAGEKAMN - 139
α7
β1 α2 β3 β4 α5 β6 α8 β9 α10 β11
N

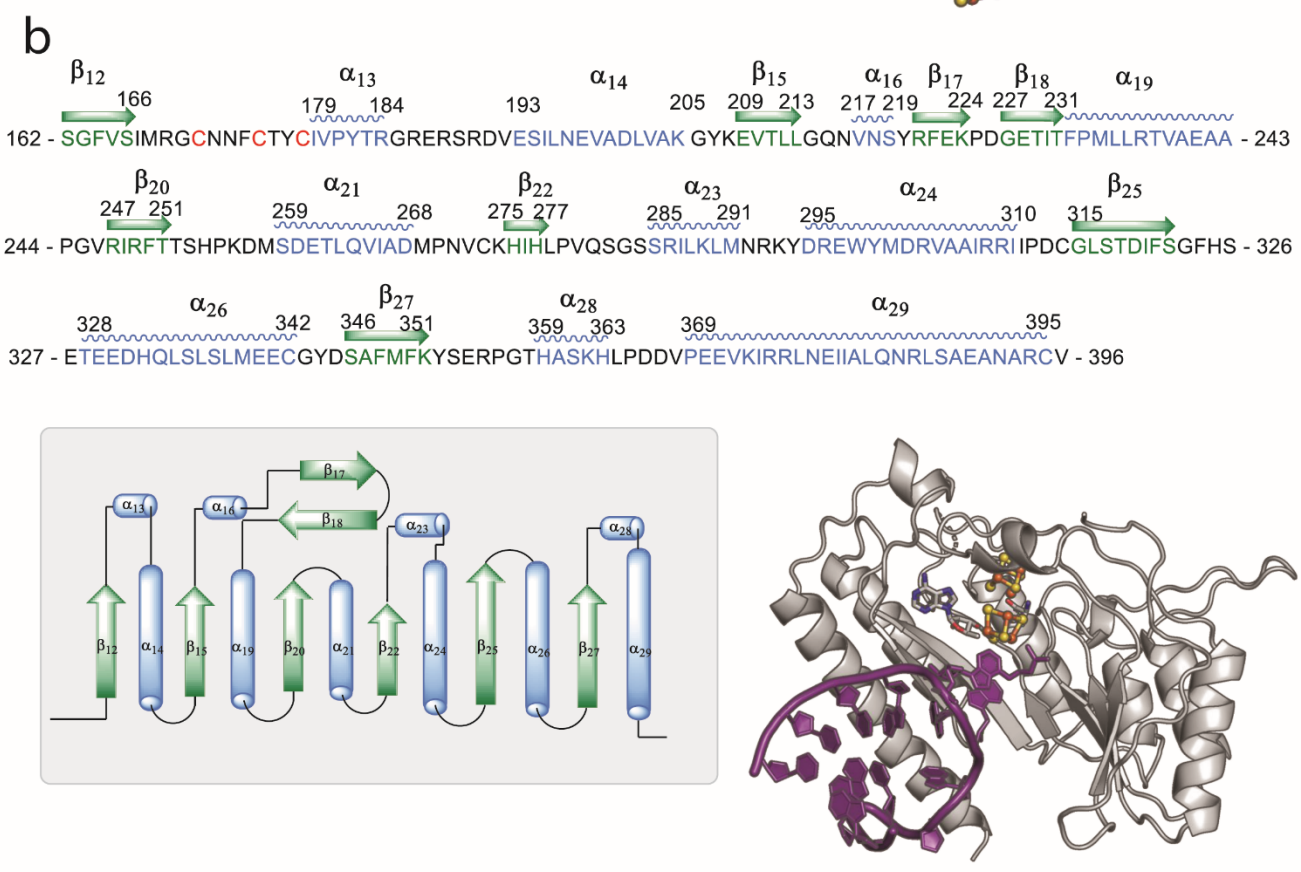
b
β12 166
α13 179 184
α14 193
β15 205 209 213
α16 217 219
β17 224
β18 227 231
α19
162 - SGFVSIMRGCNNFCTYCIVPYTRGRERSRDVESILNEVADLVAK GYKEVTLLGQNVNSYRFEKPDGETITFPMLLRTVAEAA - 243
β20 247 251
α21 259 268
β22 275 277
α23 285 291
α24 295 310
β25 315
244 - PGVRIRFTTSHPKDMSDETLQVIADMPNVCKHIHLPVQSGSSRILKLMNRKYDREWYMDRVAAIRRIIPDCGLSTDIFSGFHS - 326
α26 328 342
β27 346 351
α28 359 363
α29 369 395
327 - ETEEDHQLSLSLMEECGYDSAFMFKYSERPGTHASKHLPDDVPEEVKIRRLNEIIALQNRLSAEANARCV - 396
β17
α13
α16
β18
α23
α28
β12 α14 β15 α19 β20 α21 β22 α24 β25 α26 β27 α29

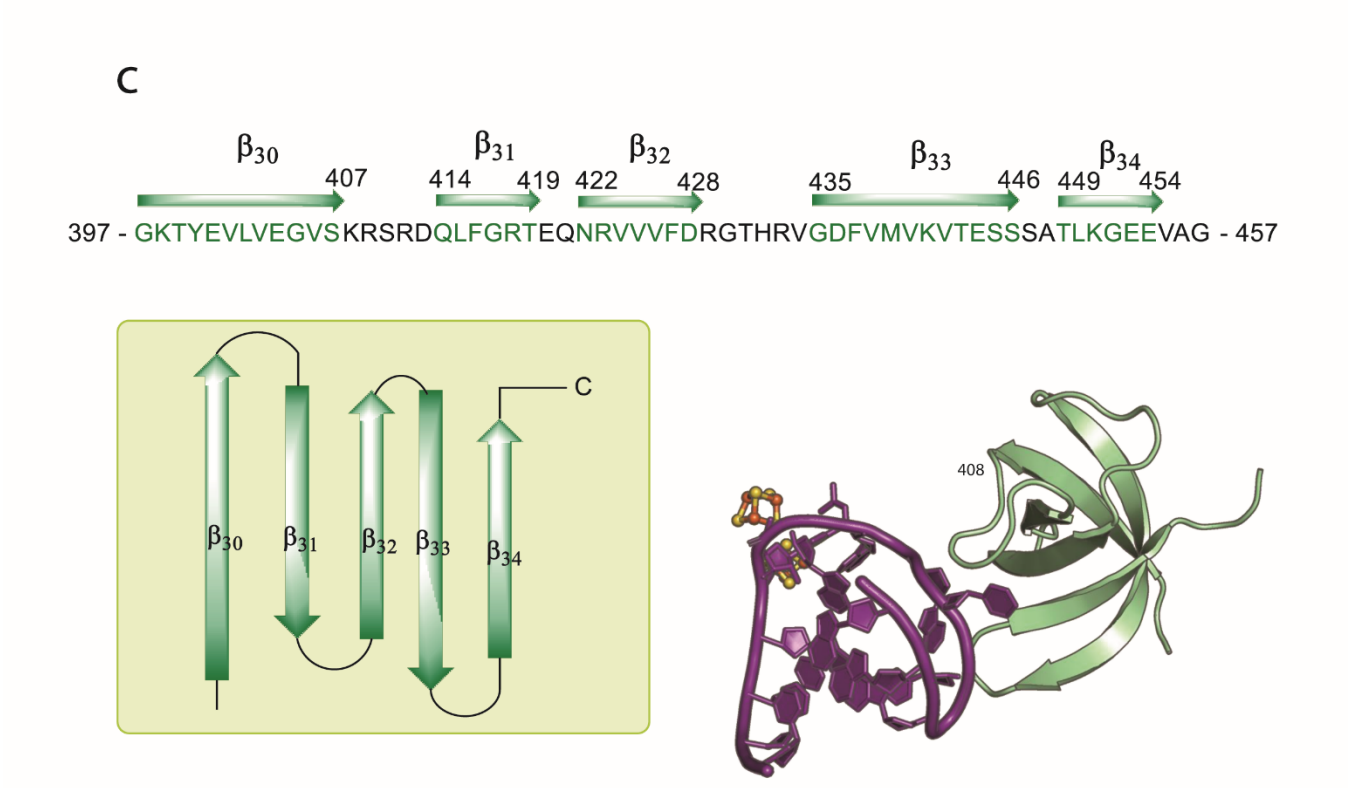

Fig. S1. Sequence, secondary structure schematic, and cartoon of the three-dimensional fold of *Bu*MiaB. **a**, N-terminal MTTase domain. **b**, radical SAM domain. **c**, C-terminal TRAM domain. Beta sheets and alpha-helices in the schematics are represented in green and blue colors respectively. The radical SAM domain exhibits a conserved core fold that consists of a shortened $(\beta\alpha)_6$ triosephosphate isomerase (TIM) barrel, and contains four short alpha helical extensions (α13, α16, α23 and α28) that make interactions with the cluster binding loop (residues from 167 to 178), as well as a solvent-exposed two-stranded β-sheet (β17- β18). All figures have the same color scheme for the domains and their associated residues: tan for MTTase, gray for radical SAM and green for TRAM. The cysteine residues involved in coordination of the clusters are colored in red.

a.

DNA

ATGGAAAAAGTTACCGGTGCCGATTTCAAAAGCGCAACCGCAGATGATAACAAAAAGCTGTTTATTGAAAC
CTACGGCTGCCAGATGAATGTTGCAGATAGCGAAGTTATTGCAAGCGTTATGCAGATGGCAGGTTATAGCG
TTGCGGATACCCTGGAAGAGGCAGATGCAGTTTTTATGAATACCTGTAGCATTCGCGATAACGCCGAACAG
AAAATTCTGAATCGTCTGGAATTTTTCCACAGCCTGAAAAAAAAGAAACGCGGTCTGATTGTTGGTGTTCT
GGGTTGTATGGCAGAACGTGTTAAAGATGATCTGATCACCAATCATCATGTGGATCTGGTTGTTGGTCCGG
ATGCATATCTGACCCTGCCGGAACTGATTGCCAGCGTTGAAGCCGGTGAAAAAGCAATGAATGTGGAACTG
AGCACCACCGAAACCTATCGTGATGTTATTCCGAGCCGTATTTGCGGTAATCATATTAGCGGTTTTGTGAG
CATTATGCGTGGCTGTAATAACTTTTGCACCTATTGCATTGTTCCGTATACACGTGGTCGTGAACGTAGCC
GTGATGTTGAAAGCATTCTGAATGAAGTTGCCGATCTGGTGGCAAAAGGTTATAAAGAAGTTACCCTGCTG
GGTCAGAATGTGAATAGCTATCGTTTTGAAAAACCGGATGGTGAAACCATTACCTTTCCGATGCTGCTGCG
TACCGTTGCCGAAGCAGCACCGGGTGTTCGTATTCGTTTTACCACCAGTCATCCGAAAGATATGAGTGATG
AAACCCTGCAGGTTATTGCAGATATGCCGAATGTGTGCAAACATATTCATCTGCCGGTTCAGAGCGGTAGC
AGCCGTATTCTGAAACTGATGAATCGTAAATATGATCGCGAGTGGTATATGGATCGTGTTGCAGCAATTCG
TCGTATTATTCCGGATTGTGGTCTGAGCACCGATATCTTTAGTGGTTTTCATAGCGAAACCGAAGAAGATC
ATCAGCTGAGCCTGAGTCTGATGGAAGAATGTGGTTATGATAGCGCCTTCATGTTCAAATATAGCGAACGT
CCGGGTACACATGCAAGCAAACATCTGCCTGATGATGTTCCGGAAGAAGTTAAAATTCGTCGCCTGAATGA
AATTATTGCCCTGCAGAATCGCCTGAGTGCGGAAGCAAATGCACGTTGTGTTGGTAAAACCTATGAAGTTC
TGGTTGAAGGTGTTAGCAAACGTTCACGTGATCAGCTGTTTGGTCGTACAGAACAGAATCGTGTTGTTGTT
TTTGATCGTGGCACCCATCGTGTGGGTGATTTTGTTATGGTTAAAGTGACCGAAAGCAGCAGCGCAACCCT
GAAAGGTGAAGAAGTTGCAGGTTAA

b.

Protein:

MEKVTGADFKSATADDNKKLFIETYGCQMNVADSEVIASVMQMAGYSVADTLEEADAVFMNTCSIRDNAEQKILNRLE
FFHSLKKKKRGLIVGVLGCMAERVKDDLITNHHVDLVVGPDAYLTLPELIASVEAGEKAMNVELSTTETYRDVIPSRI
CGNHISGFVSIMRGCNNFCTYCIVPYTRGRERSRDVESILNEVADLVAKGYKEVTLLGQNVNSYRFEKPDGETITFPM
LLRTVAEAAPGVRIRFTTSHPKDMSDETLQVIADMPNVCKHIHLPVQSGSSRILKLMNRKYDREWYMDRVAAIRRIIP
DCGLSTDIFSGFHSETEEDHQLSLSLMEECGYDSAFMFKYSERPGTHASKHLPDDVPEEVKIRRLNEIIALQNRLSAE
ANARCVGKTYEVLVEGVSKRSRDQLFGRTEQNRVVVFDRGTHRVGDFVMVKVTESSSATLKGEEVAG*

Fig. S2. *Bu*MiaB DNA and protein sequences for structures with substrates. a, DNA sequence. **b**, Protein sequence. Note that His363 (shown in red) is Y363 in the native *Bu*MiaB structure